Supplementary Information

Composition-Property Relationships of Choline Based Eutectic Solvents: Impact of the Hydrogen Bond Donor and CO_2 Saturation

Ruth Dikki[1], Vaishali Khokhar[1], Muhammad Zeeshan[1], Sanchari Bhattacharjee[2], Oguz Kagan Coskun[1], Rachel Getman[2,3], Burcu Gurkan[1,*]

[1] Department of Chemical and Biomolecular Engineering, Case Western Reserve University, Cleveland, OH 44106

[2] Department of Chemical and Biomolecular Engineering, Clemson University, Clemson, SC 29634-0909 USA

[3] Current address: William G. Lowrie Department of Chemical and Biomolecular Engineering, The Ohio State University, Columbus, OH 43210 USA

[*] Corresponding: beg23@case.edu

Table of Contents (31 pages)

17 Figures

8 Tables

MATERIALS AND METHODS

Materials

The precursors used in the synthesis of HBAs include imidazole (ImH) (99%, Thermo Scientific), 1,2,4-triazole (TrzH) (98%, Sigma-Aldrich), pyrrole-2-carbonitrile (CNpyrH) (99%, Alfa Aesar), phenol (PhOH) (98%, Sigma-Aldrich), and choline chloride (99%, Sigma-Aldrich). Ethylene glycol (99.8%, Sigma-Aldrich) and ethanolamine (>99%, TCI) HBDs were used as received, whereas 1,2-propylene glycol (≥ 99.0%, Sigma-Aldrich) was dried with molecular sieves (Metrohm; 0.3 nm dia.), activated by heating at 150 °C for 24 hours prior to use. Other synthesis and characterization materials include the hydroxide-form anion exchange resin (A600-OH, Purolite), xylene (≥98.5%, Thermo Scientific), silver nitrate (0.171N, Ricca), methanol (99.8%, HPLC grade, Fischer), and deuterated dimethyl sulfoxide-d6 (DMSO-d6, 99.9%). The absorbance probes, 4-nitroaniline (NA) (99%, Sigma-Aldrich), *N,N*-diethyl-4-nitroaniline (DENA) (97%, Oakwood Chemicals) and betaine dye 30 (Toronto Research Chemicals) were used as received.

Experimental

Synthesis and characterization

The synthesis of the HBAs shown in **Table 1** is described previously[1]. Briefly, $[\mathrm{Ch}]^+[\mathrm{Cl}]^-$ was dissolved in methanol and converted to choline hydroxide ($[\mathrm{Ch}]^+[\mathrm{OH}]^-$) via anion exchange. Then, equimolar amount of ImH, PhOH, CNpyrH, and TrzH were added to the $[\mathrm{Ch}]^+[\mathrm{OH}]^-$ solution in methanol for acid-base neutralization reaction. Finally, the excess methanol was removed by rotary evaporation, and the obtained products further dried at 50 °C under vacuum on a Schlenk line. It was found that a proton sharing equilibrium exists as illustrated in **Table 1** for $\mathrm{Ch}^{\pm}\mathrm{ImH} \,/\, [\mathrm{Ch}]^+[\mathrm{Im}]^-$ and $\mathrm{Ch}^{\pm}\mathrm{PhOH} \,/\, [\mathrm{Ch}]^+[\mathrm{PhO}]^-$, as confirmed previously by nuclear magnetic resonance (NMR), Fourier transform infrared spectroscopy (FTIR), and density

functional theory (DFT) calculations.[1] Experimentally, when completely dried, the formation of $Ch^{\pm}$ and ImH or PhOH is favored over the formation of $[Ch]^{+}$ and $[Im]^{-}$ or $[PhO]^{-}$. The synthesized HBAs were further mixed with EG, PG, and MEA at 40 °C according to 1:2 HBA:HBD molar ratios to obtain the eutectic solvents. Samples were characterized, and successful synthesis confirmed, by ^{1}H and ^{13}C NMR (Bruker 500 MHz) (Figures S4-S8) and attenuated total reflectance-Fourier transform infrared spectroscopy (ATR-FTIR) (Nicolet iS50 FTIR, Thermo Scientific). DSC (Mettler Toledo DSC3) measurements were performed by first heating the samples from 25 °C to 40 °C at a rate of 10 °C/min and then cooling to -150 °C at the same rate before reheating back to 40 °C. The second heating curve is reported for each sample. TGA (TGA500, TA instruments) measurement was performed to examine the thermal stability of the eutectic solvents. For this, samples were first treated at 40 °C for 15 minutes and then heated to 300 °C at 10 °C/min under nitrogen. The reported onset temperatures (T_{onset}) correspond to the temperature where 5% mass loss occurred. For determining the rate of mass loss due to evaporation at temperatures typical for regenerating the solvents after saturation with CO_2, isothermal TGA experiments were performed at 50 °C where the samples were placed under nitrogen flow at 100 mL/min for 60 minutes.

Physical properties

Density. The temperature-dependent densities of the liquid samples were measured between the temperature range of 25 - 50 °C using a U-tube density meter (DMA-T500, Anton-Paar) with a ±0.00001 g/cm^3 uncertainty. Whereas the densities of the solid HBAs were measured at 25 °C using a 10 cm^3 pycnometer. For this measurement, about 0.3 g of the solid HBA was added into the pycnometer and xylene (in which HBAs are not soluble) was added up to fill. The density of the solid HBA was then estimated using eqn. S1, where ρ, *m*, and *v* stand for density, measured

mass, and volume, respectively, and the subscripts *s* and x stand for solid HBA and xylene, respectively. To confirm the accuracy of this technique, the pycnometer was first tested with imidazole with a known density of 1.23 g/cm^3 at 25 °C,[2] and observed to have an accuracy of ±4%.

$$\rho_s = \frac{m_s}{v_s} \text{ , where } v_s = 10 \text{ cm}^3 - \frac{m_x}{\rho_x} \quad \text{(S1)}$$

The dependence on temperature of the measured densities of the eutectic solvents was obtained from the linear fit equation shown in eqn. S2, where ρ (g/cm^3) and T (K) represents the densities and temperatures of the eutectic solvents, while A and B represent the fit parameters.

$$P = A * T * 10^{-4} + B \quad \text{(S2)}$$

Eqn. S3 further shows the expression used to calculate the excess molar volumes (V_m^E) from the density values of the HBAs, HBDs, and the eutectic solvents obtained at 25 °C. M_i (g), ρ_i (g/cm^3), and x_i represent the molecular weight, density, and mole fraction of component i, while ρ represents the density of the eutectic solvents.

$$V_m^E = \Sigma_i \left(\frac{1}{\rho} - \frac{1}{\rho_i}\right) M_i x_i \quad \text{(S3)}$$

Viscosity. The viscosities of the liquid samples were measured using a microchannel viscometer (μVISC, Rheosense) with an uncertainty of ±5% between the temperature range of 25 - 50 °C. The measured viscosities were fitted to the Vogel–Fulcher–Tammann (VFT) expression in eqn. S4 to express the viscosity with respect to the glassy behavior of the eutectics. Here η_0, C, and To represent the fit parameters, while T and η represent the temperature (K) and viscosity (mPa.s), respectively.

$$\text{In}(\eta) = \text{In}(\eta_0) + \left(\frac{C}{T - T_O}\right) \quad \text{(S4)}$$

Ionic Conductivity. Electrochemical impedance spectroscopy (EIS) was employed to determine the conductivity of the eutectic solvents. The solvents were placed in a cell with dual platinum electrodes (MMA 500, Materials Mates Italia). The impedance measurements were performed using BioLogic SP-240 potentiostat equipped with frequency response analyzer (7 MHz to 10 μHz). To control the temperature for conductivity measurements, the cell was enclosed in the RheoSense MicroVISC Temperature Control unit (±0.10 K). The solution resistance was deduced from the intercept of a linear fit to the capacitive region of the Nyquist plot (imaginary versus real impedance). This resistance value was then used to calculate conductivity using eqn. S5:

$$\sigma\ (\mathrm{mS.cm^{-1}}) = \frac{k\ (cm^{-1})}{\rho\ (ohm)} \times 1000 \qquad \text{(S5)}$$

where σ denotes the conductivity, k is the cell constant, and ρ is the solution resistance. The estimated standard uncertainty is given by u(σ) = 0.05. Similar to temperature-dependent viscosities, VFT model was employed to fit the conductivity data:

$$\sigma = \sigma_0 \times e^{-D/T-T_0} \qquad \text{(S6)}$$

where σ_0 (mS.cm^{-1}) signifies the conductivity at an infinitely high temperature, and D (K) and T_0 (K) are fit parameters.

Solvatochromic studies

The stock solutions of the NA, DENA, and Betaine 30 were prepared by dissolving the requisite amount of respective probe weighed (±0.1 mg) in absolute ethanol. The stock solutions were stored under refrigeration in amber-colored glass vials. For sample preparation, the pre-calculated amount of the probe solution from the stock was transferred to the glass vials and ethanol was evaporated under gentle stream of air. The pre-determined amount of respective eutectic solvent was added to the vials to achieve the desired probe concentration (30 μM for NA and DENA while 100 μM for

betaine dye 30). To ensure complete re-dissolution of the probe molecule the sample solutions were thoroughly mixed by a combination of intermittent vortexing and gentle heating. The samples were transferred to the quartz cuvette and UV-Vis absorbance spectra of all samples were obtained using Agilent Cary 3500 Peltier double beam UV-Vis Spectrometer over 200 nm to 800 nm spectral range. The empirical Kamlet-Taft parameters, dipolarity/polarizability (π*), H-bond accepting (HBA) basicity (β), E_T(30), and H-bond donating (HBD) acidity (α) were determined from the absorbance response of the above-mentioned dyes using the following equations,

$$\pi^* = (27.52\text{-}\bar{\upsilon}_{DENA})\times 0.314 \quad \text{(S7)}$$

$$\beta = \frac{1.035\bar{\upsilon}_{DENA} - \bar{\upsilon}_{NA} + 2.64}{2.8} \quad \text{(S8)}$$

$$E_T(30) = 28591.5/\lambda_{max}\,(\text{nm}) \quad \text{(S9)}$$

$$\alpha = \frac{[E_T(30) - 14.6(\pi^* - 0.23\delta - 30.31)]}{16.5} \quad \text{(S10)}$$

where $\bar{\upsilon}_{DENA}$ and $\bar{\upsilon}_{NA}$ represents the absorbance maxima for DENA and NA in kK units (1000 cm^{-1} = 1 kK, and λ_{max} is the lowest energy absorbance maxima for betaine dye 30 of the respective samples). δ is a polarizability parameter defined as 0.00 for all nonhalogenated aliphatic solvents, 0.50 for all polyhalogenated aliphatic, and 1.00 for all aromatic solvents.

Electrochemical stability

Cyclic voltammetry (CV) experiments were carried out utilizing a three-electrode setup with the BioLogic VSP-300 electrochemical station to assess the electrochemical characteristics of neat eutectic solvents. Prior to each set of these measurements, the uncompensated solution resistance was measured and subsequently corrected for iR drop at 85% using positive feedback through the EC-Lab software (V11.42, BioLogic). The working electrode consisted of a Pt microelectrode (10

mm dia., BASi), the counter electrode was composed of glassy carbon (3 mm dia., BASi) and a Pt wire (1 mm dia.) with ferrocene (10 mM) dissolved in the electrolyte served as the quasi-reference electrode (QRE) and internal reference, respectively. The electrochemical cell adopted a T-cell configuration, and a continuous N_2 (99.999%, Airgas) atmosphere was maintained throughout the voltammetry studies to ensure an oxygen- and humidity-free atmosphere.

Prior to recording CVs, the open circuit potential (OCP) was measured for 30 minutes to allow the system to relax and the OCP to stabilize. Initially, CVs were recorded by sweeping the potential window from -0.5 V to +1 V vs. QRE to identify the ferrocene peak position, employing a scan rate of 1000 $mV.s^{-1}$ (see Figure S15). Subsequently, the electrochemical window was extended from -2.5 V to +2.5 V vs. Fc/Fc^+ to explore the upper and lower limits of the electrochemical windows of the investigated eutectic solvents. For these investigations, a scan rate of 10 $mV.s^{-1}$ was employed.

CO_2 absorption experiments

CO_2 absorption experiments were performed gravimetrically at 1 bar of CO_2 and 25 °C following our previous report.[1] Accordingly, about 0.5/1.2 g of sample was placed in a 3 mL vial and CO_2 was bubbled through it at a flow rate of 20 mL/min (controlled with a mass flow controller 5850I, Brooks) while stirring at about 300 rpm. The weight of the setup was recorded every 5 mins with a gravimetric balance (±0.1 mg) until complete CO_2 saturation. Equilibrium in CO_2 saturation was verified through stable mass over four consecutive weighing measurements.

Computational

Quantitative structure-property relationship (QSPR) analysis

The molecular descriptors needed for the QSPR analysis were calculated for the individual components of the eutectic solvents (i.e., HBA cation, HBA anion, and the neutral HBD molecule) using density functional theory (DFT). First, the geometry optimization of the molecular structures was performed by employing the Becke's three parameter hybrid exchange functional and the Lee–Yang–Parr correlation function (B3LYP, 6-311++G** basis set) using the Spartan 14 Parallel Suite (Wavefunction Inc., version 1.1.4). The following structural descriptors were considered for QSPR modeling (numerical values are summarized in Table S7 and S8): energy of the highest occupied molecular orbital (E HOMO) (eV), energy of the lowest un-occupied molecular orbital (E LUMO) (eV), dipole (debye), CPK (space filling model) area (Å²), polar surface area (PSA) (Å²), CPK volume (Å³), CPK ovality, polarizability, HBD Count, HBA count, zero-point energy (ZPE) (kJ/mol), entropy (S°) (J/mol°), enthalpy (H°) (au), Gibbs energy (G°) (au), and constant volume heat capacity (Cv) (J/mol°). Enhanced replacement method (ERM) algorithm in MATLAB (R2022b, 9.12.0.2080170) was employed to find the optimum set of structural descriptors to derive a linear mathematical expression. Eqn. S11 shows the general model applied for correlating descriptors separately to the CO_2 capacities, densities, and viscosities of the eutectic solvents.

$$Y(model) = b_0 + \sum_{i=1}^{n} a_i x_i \quad \text{(S11)}$$

Y represents the dependent model variable (i.e., capacity, density, or viscosity) of the eutectic solvents, b_0 and a_i the regression constant and coefficient, respectively, and x_i the parameters of the structural descriptor.

Molecular dynamics (MD) simulations

MD simulations were performed on models of $[Ch]^+[Trz]^-$, $[Ch]^+[CNpyr]^-$, $Ch^{\pm}ImH$, and $Ch^{\pm}PhOH$ using the Gromacs 5.1.4 software.[3] The molecular structures of the studied systems are shown in Figure S9. While experimental systems considered systems where proton transfer is present, simulated systems instead considered zwitterion choline $Ch^{\pm}$. This choice is significantly more computationally tractable but could impact the precision of our findings in systems where proton transfer dictates the observed phenomena. Simulation boxes with dimensions 6.0 × 6.0 × 6.0 nm^3 were employed. Molecules were added to the system using PACKMOL[4] using 200 cations ($[Ch]^+$ or $Ch^{\pm}$) and 200 anions ($[Trz]^-$, $[CNpyr]^-$, ImH, or PhOH) with 400 HBDs (EG, PG, MEA). Initial structures and molecular topologies were obtained from the automated topology builder (ATB).[5] Energy minimization using the steepest-descent method was performed to relax the forces in the system, as well as to remove any unfavorable contacts in the initial structure. This was accompanied by the equilibration of all systems in the canonical (NVT) ensemble for a duration of 2 ns, which was then followed by a 35 ns simulation in isothermal-isobaric (NPT) ensemble. Production runs in the NPT ensemble lasted for 20 ns (the last 10 ns were used for analysis from trajectories saved every 0.4 ps). During the production run, the temperature and pressure were controlled using the Nose-Hoover thermostat[6] and Parrinello-Rahman barostat[7] respectively. The equations of motion were integrated using the velocity verlet algorithm with a time step of 0.001 ps. The GROMOS54A7[8] force field was employed. This force field includes both bonded and non-bonded interactions. The full set of parameters is available on our GitHub page (https://github.com/getman-research-group/DES-FF). The non-bonded interactions were modelled using Lennard-Jones and Coulomb potentials to a cut-off of 12 Å. Long range corrections were applied for the Lennard-Jones interactions, while the Particle Mesh Ewald (PME) summation

technique[6] was employed to handle electrostatic interactions beyond the cut-off. All the bonds involving H-atoms were kept rigid using the LINCS algorithm.[9] Using these parameters, simulated densities were observed to be in good agreement with the experimental densities as seen in Table S2 The number of hydrogen bonds (HBs) were calculated for every frame in the last 10 ns of the NVT trajectories using the *hbond module* in Gromacs 5.1.4 software[3] using the criteria that the acceptor-donor atom distance is less than or equal to 3.5 Å, and the angle Acceptor atom–Donor atom–Hydrogen is than 30 degrees. The centre of mass (COM) radial distribution functions (RDFs) was generated using 5000 configurations from the last 10 ns of the NVT trajectories.

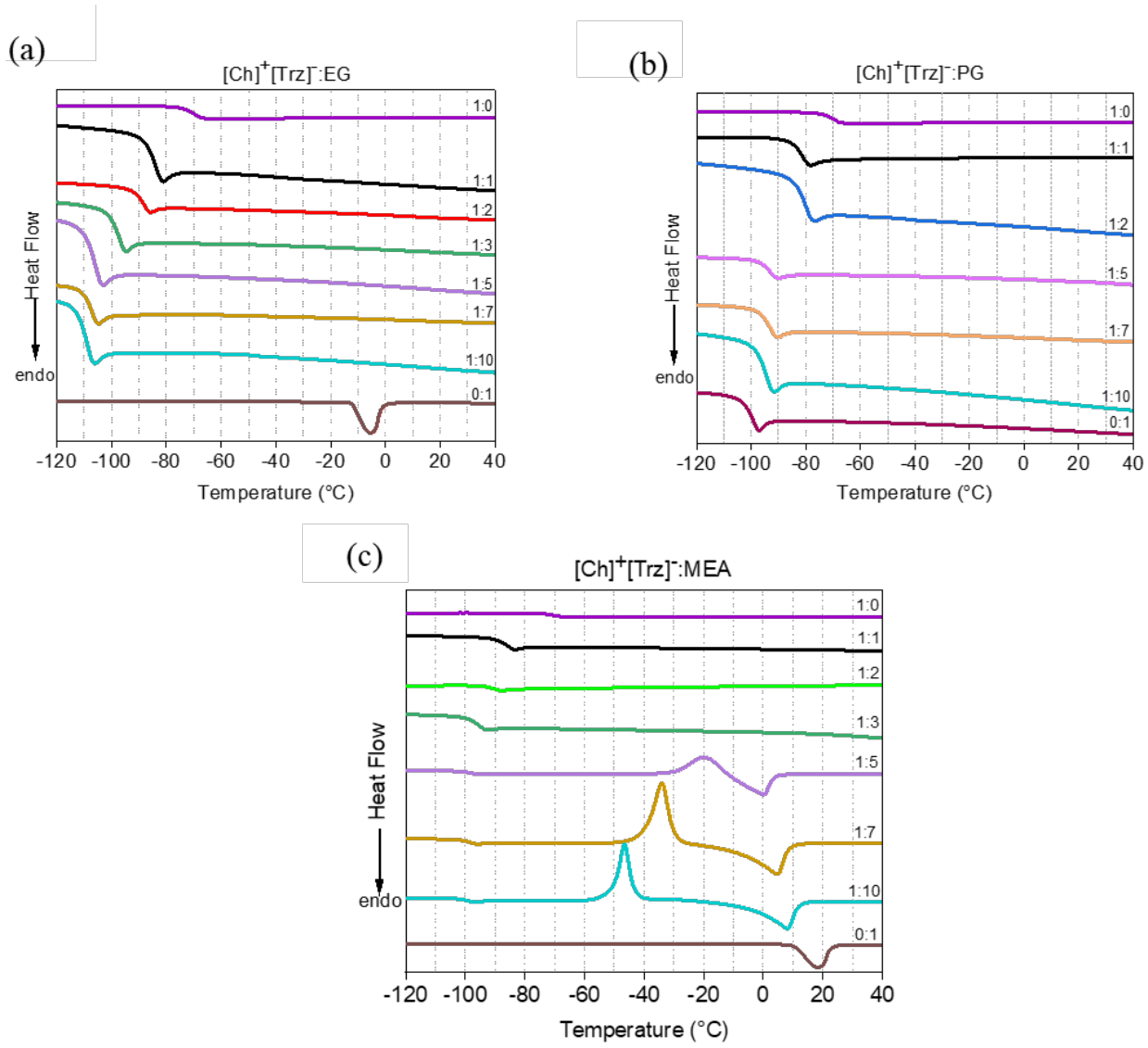

Figure S1. DSC thermogram of $[Ch]^+[Trz]^-$ based eutectic solvents with different molar ratios of ethylene glycol (EG) (a), 1,2-propylene glycol (PG) (b), and monoethanolamine (MEA) (c) in the eutectic solvents.

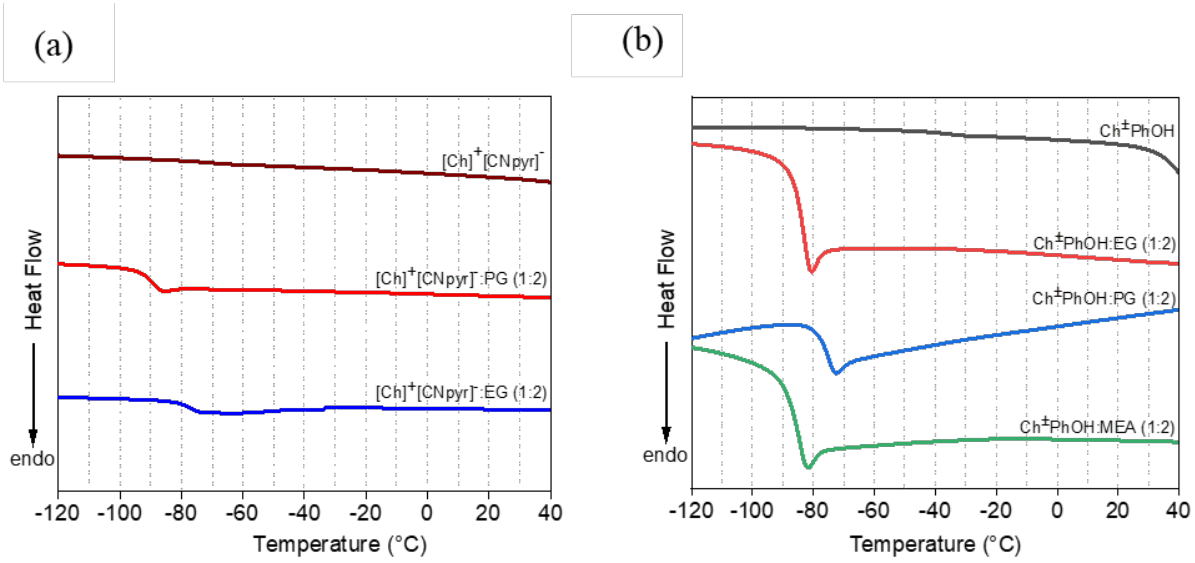

Figure S2. DSC thermograms of $[Ch]^+[CNpyr]^-$ (a) and $Ch^{\pm}PhOH$ (b) based eutectic solvent with EG, PG, and MEA (for $Ch^{\pm}PhOH$ alone) HBDs.

Table S1. Impact of the boiling point of the HBDs on the onset degradation temperatures of the eutectic solvents. Note: $T_{0.05}$ represents the onset degradation temperature where 5% mass loss occurred.

HBD		HBA		HBA:HBD (1:2)
	Boiling point (°C)		$T_{0.05}$ (°C)	$T_{0.05}$ (°C)
EG	197[10]	$Ch^{\pm}ImH$	140[1]	129[1]
		$Ch^{\pm}PhOH$	141[1]	116[1]
		$[Ch]^+[CNpyr]^-$	165[1]	107[1]
		$[Ch]^+[Trz]^-$	167[1]	115[1]
PG	187[11]	$Ch^{\pm}ImH$	140	111
		$Ch^{\pm}PhOH$	141	98
		$[Ch]^+[CNpyr]^-$	165	95
		$[Ch]^+[Trz]^-$	167	113
MEA	171[12]	$Ch^{\pm}ImH$	140	91
		$Ch^{\pm}PhOH$	141	102
		$[Ch]^+[Trz]^-$	167	87

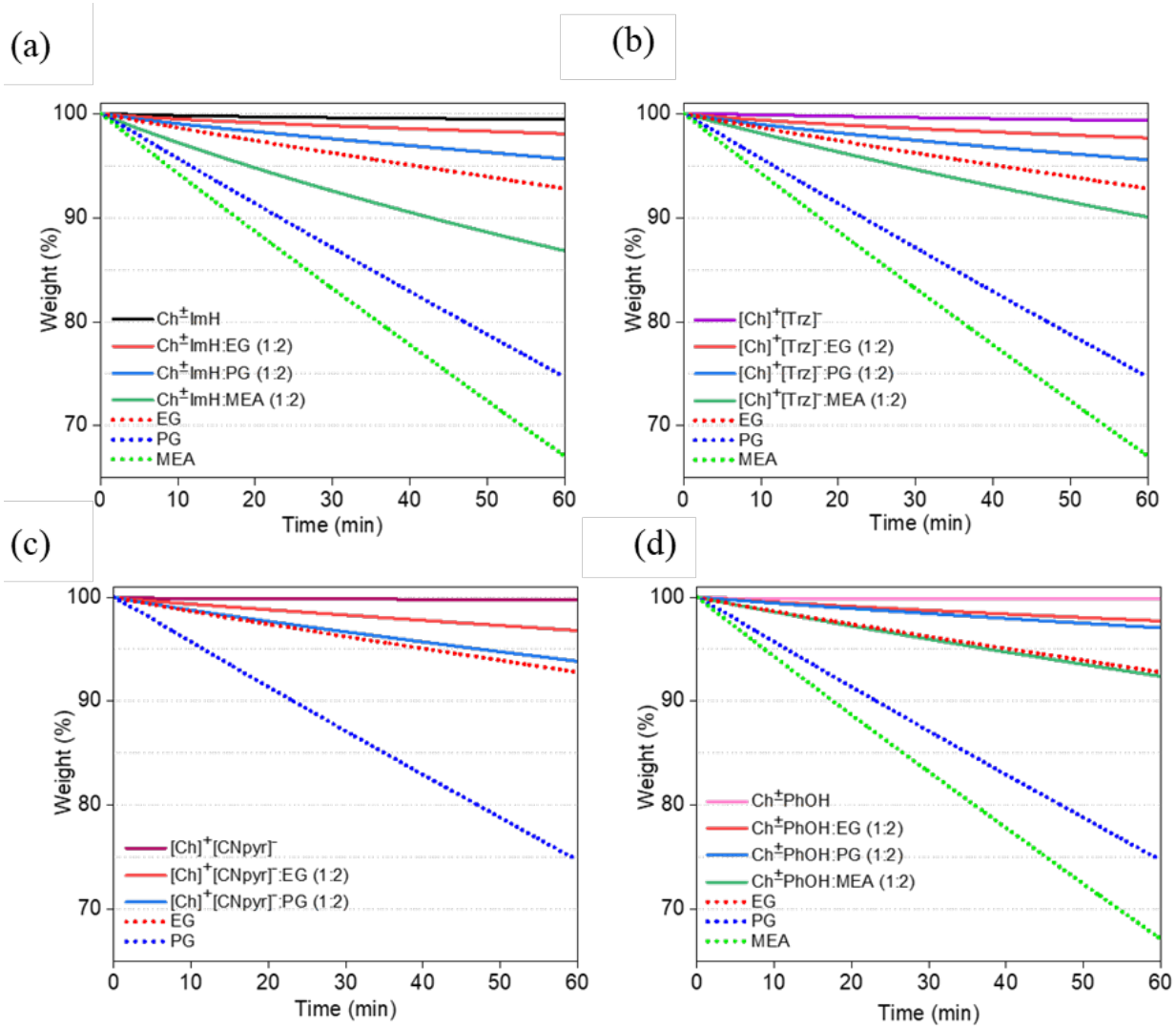

Figure S3. TGA isothermal curves for $Ch^{\pm}ImH$ (a), $[Ch]^{+}[Trz]^{-}$ (b), $[Ch]^{+}[CNpyr]^{-}$ (c), and $Ch^{\pm}PhOH$ (d) HBAs with their corresponding eutectic solvents.

Table S2. Simulated and experimental densities of the eutectic solvents at 25 °C, with water content as measured by KF titrator.

	Simulated Density (g/cm^3)	Experimental Density (g/cm^3)	% Difference	Water content (ppm)
$Ch^{\pm}$PhOH:EG (1:2)	1.147±0.01	1.10333	3.96	3600
$Ch^{\pm}$PhOH:PG (1:2)	1.115±0.12	1.06866	4.34	2700
$Ch^{\pm}$PhOH:MEA (1:2)	1.021±0.08	1.05834	3.53	1900
$Ch^{\pm}$ImH:EG (1:2)	1.115±0.09	1.10043	1.32	5200
$Ch^{\pm}$ImH:PG (1:2)	1.088±0.04	1.06502	2.16	8900
$Ch^{\pm}$ImH:MEA (1:2)	0.987±0.02	1.05380	6.34	-
$[Ch]^{+}[Trz]^{-}$:EG (1:2)	1.164±0.11	1.12096	3.84	5200
$[Ch]^{+}[Trz]^{-}$:PG (1:2)	1.137±0.08	1.08484	4.81	5500
$[Ch]^{+}[Trz]^{-}$:MEA (1:2)	1.009±0.08	1.07822	6.42	6800
$[Ch]^{+}[CNpyr]^{-}$:EG (1:2)	1.138±0.12	1.09477	3.95	3800
$[Ch]^{+}[CNpyr]^{-}$:PG (1:2)	1.112±0.09	1.06229	4.68	2960

Table S3. Fitting parameters for density.

Sample	$P\ (\frac{g}{cm^3}) = A * T\ (K) * 10^{-4} + B$	
	A	B
$Ch^{\pm}$ImH:EG (1:2)	-5.9240	1.2770
$Ch^{\pm}$PhOH:EG (1:2)	-5.8423	1.2774
$[Ch]^{+}[CNpyr]^{-}$:EG (1:2)	-6.4840	1.2881
$[Ch]^{+}[Trz]^{-}$:EG (1:2)	-5.9429	1.2980
$Ch^{\pm}$ImH:PG (1:2)	-6.1023	1.2469
$Ch^{\pm}$PhOH:PG (1:2)	-6.0309	1.2484
$[Ch]^{+}[CNpyr]^{-}$:PG (1:2)	-6.4389	1.2542
$[Ch]^{+}[Trz]^{-}$:PG (1:2)	-6.0743	1.2659
$Ch^{\pm}$ImH:MEA (1:2)	-6.2754	1.2408
$Ch^{\pm}$PhOH:MEA (1:2)	-6.2006	1.2431
$[Ch]^{+}[Trz]^{-}$:MEA (1:2)	-6.5503	1.2734

Table S4. Fitting parameters for viscosity according to the VFT model.

Sample	$\ln(\eta) = \ln(\eta_o) + \left(\frac{C}{T - T_O}\right)$			
	η_o (mPa.)	C (K)	T_O (K)	R^2
$Ch^{\pm}$ImH:EG (1:2)	0.0295	1281.90	152.60	0.9997
$Ch^{\pm}$PhOH:EG (1:2)	0.0146	1574.47	142.20	0.9999
$[Ch]^+[CNpyr]^-$:EG (1:2)	0.0142	1302.19	150.63	0.9996
$[Ch]^+[Trz]^-$:EG (1:2)	0.0401	1188.75	155.96	0.9991
$Ch^{\pm}$ImH:PG (1:2)	0.0376	1160.63	171.51	0.9996
$Ch^{\pm}$PhOH:PG (1:2)	0.0135	1509.17	157.45	0.9999
$[Ch]^+[CNpyr]^-$:PG (1:2)	0.0070	1500.61	149.14	0.9997
$[Ch]^+[Trz]^-$:PG (1:2)	0.0170	1377.59	158.58	0.9997
$Ch^{\pm}$ImH:MEA (1:2)	0.0670	922.52	175.53	0.9993
$Ch^{\pm}$PhOH:MEA (1:2)	0.2161	698.46	194.86	0.9997
$[Ch]^+[Trz]^-$:MEA (1:2)	0.0106	1492.21	137.80	0.9991

Table S5. Fitting parameters associated with ionic conductivity according to the VFT model.

Solvent	$\ln(\sigma) = \ln(\sigma_0) - \left(\frac{D}{T - T_0}\right)$			
	σ_0 (mS/cm)	D (K)	T_0 (K)	R^2
$Ch^{\pm}$ImH:EG (1:2)	3270.36	1093.52	152.60	0.9998
$Ch^{\pm}$PhOH:EG (1:2)	4911.86	1365.92	142.20	0.9996
$[Ch]^+[CNpyr]^-$:EG (1:2)	4582.56	1120.37	150.63	0.9992
$[Ch]^+[Trz]^-$:EG (1:2)	2420.48	1047.58	155.96	0.9952
$Ch^{\pm}$ImH:PG (1:2)	2171.47	1026.02	171.51	0.9999
$Ch^{\pm}$PhOH:PG (1:2)	2385.49	1234.85	157.43	0.9997
$[Ch]^+[CNpyr]^-$:PG (1:2)	7535.34	1320.58	149.13	0.9998
$[Ch]^+[Trz]^-$:PG (1:2)	2848.03	1159.69	158.58	0.9994
$Ch^{\pm}$ImH:MEA (1:2)	1132.07	826.39	175.53	0.9997
$Ch^{\pm}$PhOH:MEA (1:2)	377.36	633.61	194.86	0.9994
$[Ch]^+[Trz]^-$:MEA (1:2)	4632.03	1260.80	137.80	0.9951

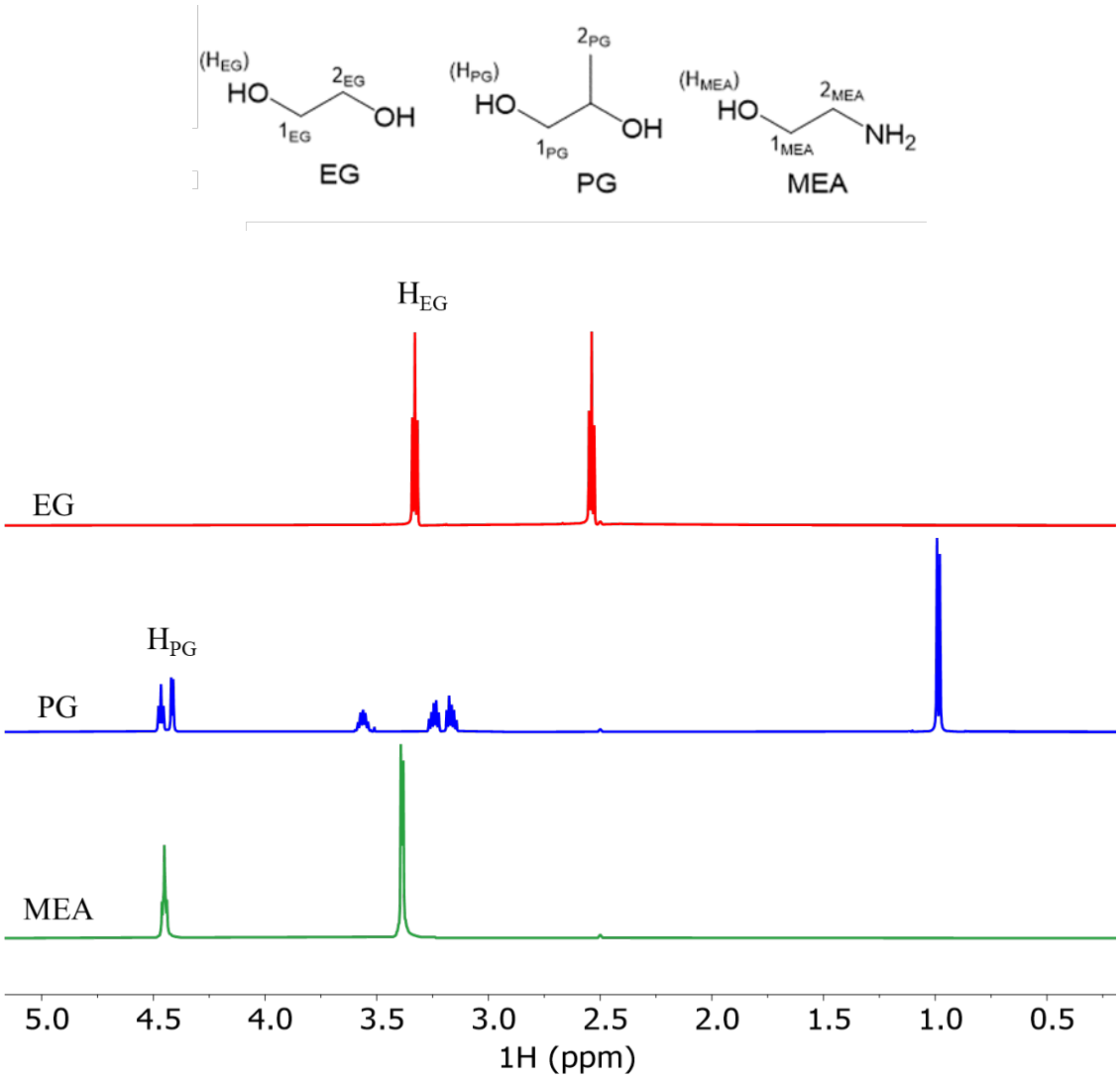

Figure S4. ^{1}H-NMR spectra of neat EG, PG, and MEA HBDs in DMSO-d6.

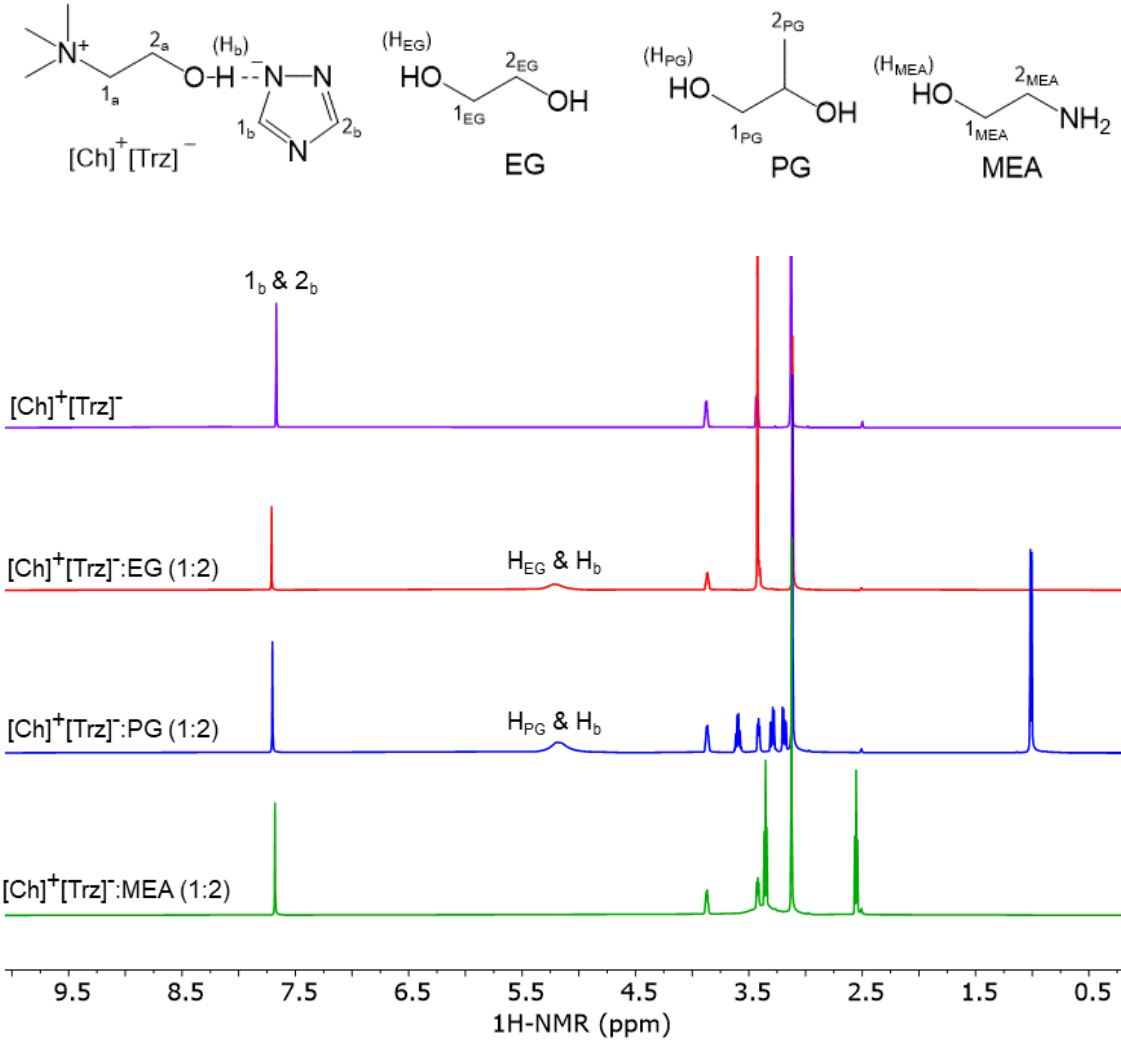

Figure S5. ^{1}H-NMR spectra of $[Ch]^{+}[Trz]^{-}$ based eutectic solvents with EG, PG, and MEA HBDs in DMSO-d6.

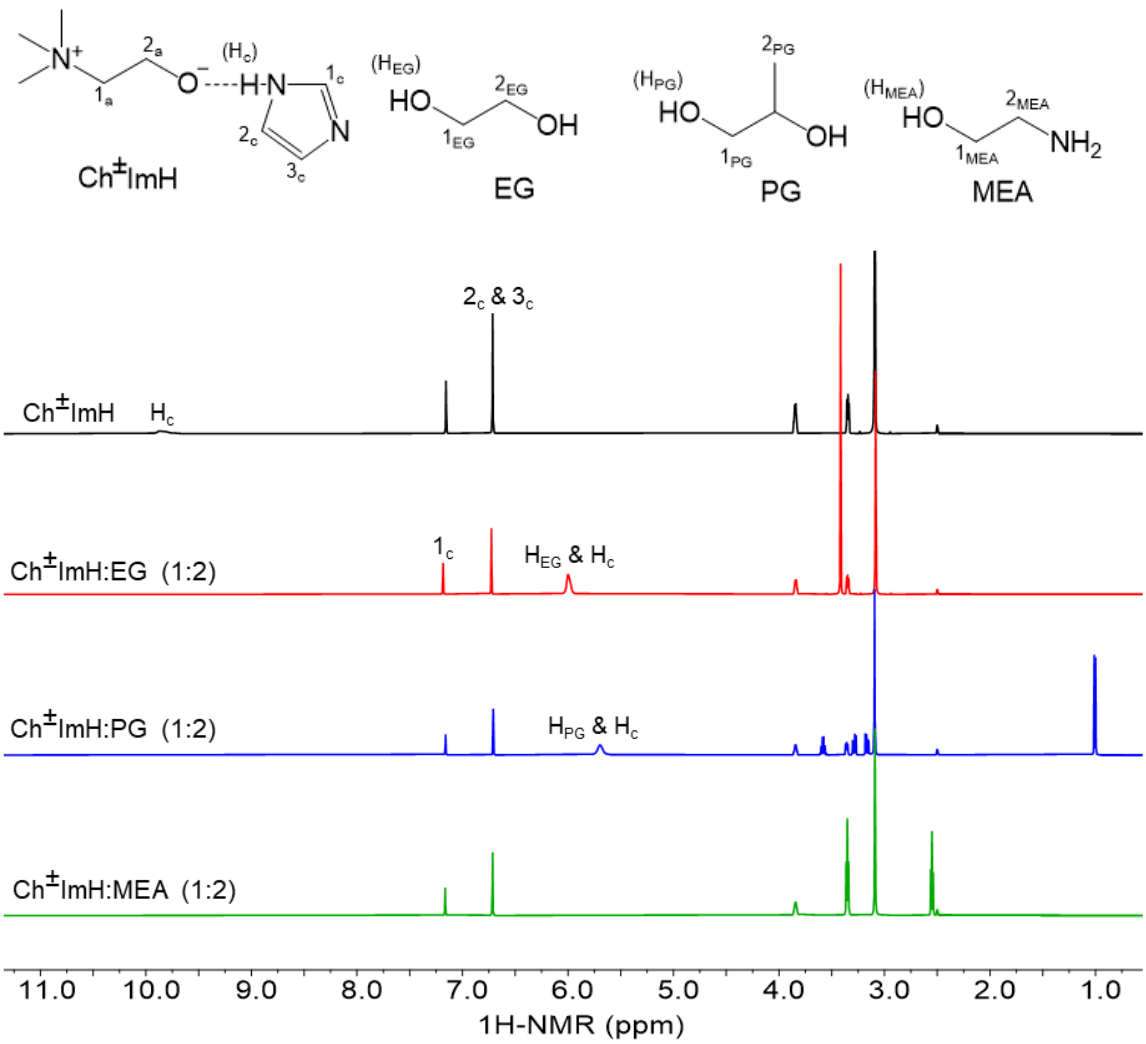

Figure S6. ^{1}H-NMR spectra of Ch$^{\pm}$ImH based eutectic solvents with EG, PG, and MEA HBDs in DMSO-d6.

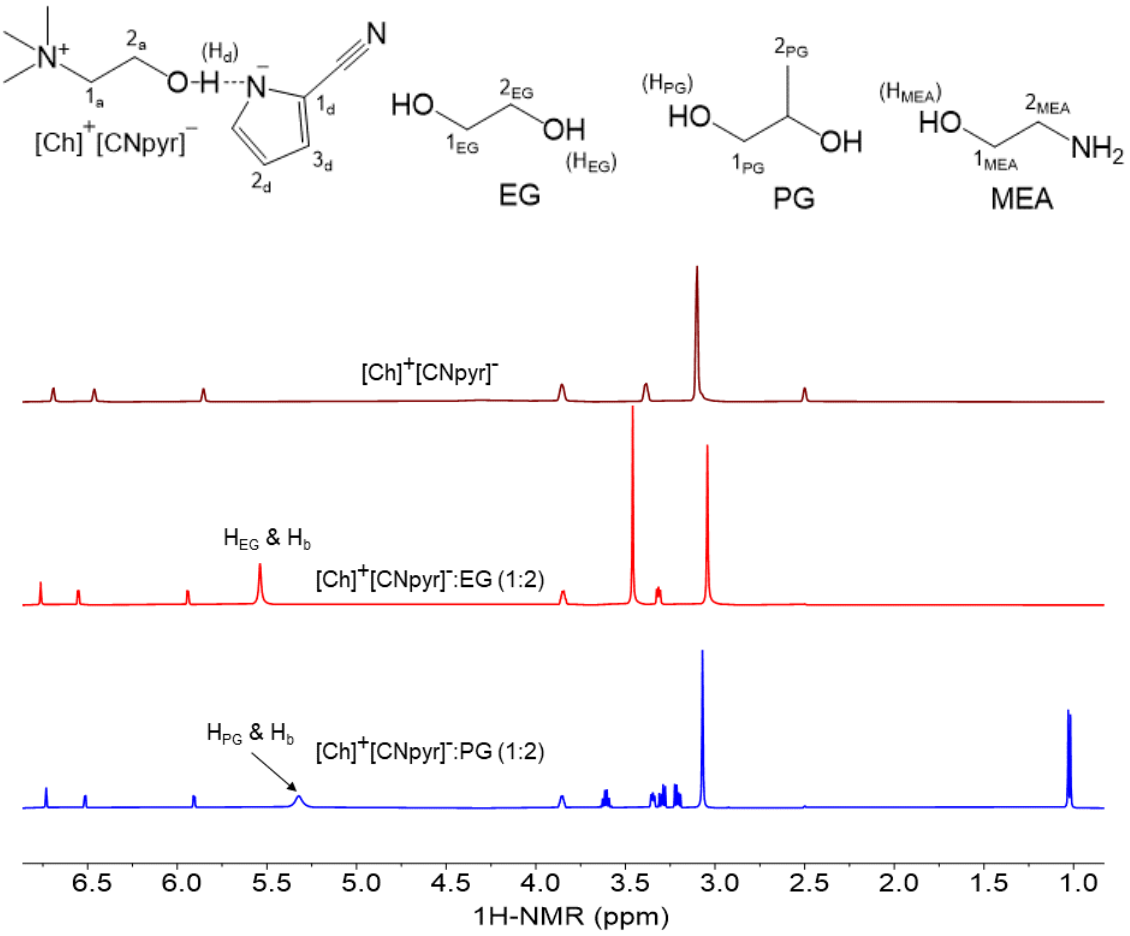

Figure S7. ^{1}H-NMR spectra of $[Ch]^{+}[CNpyr]^{-}$ based eutectic solvents with EG, PG, and MEA HBDs in DMSO-d6

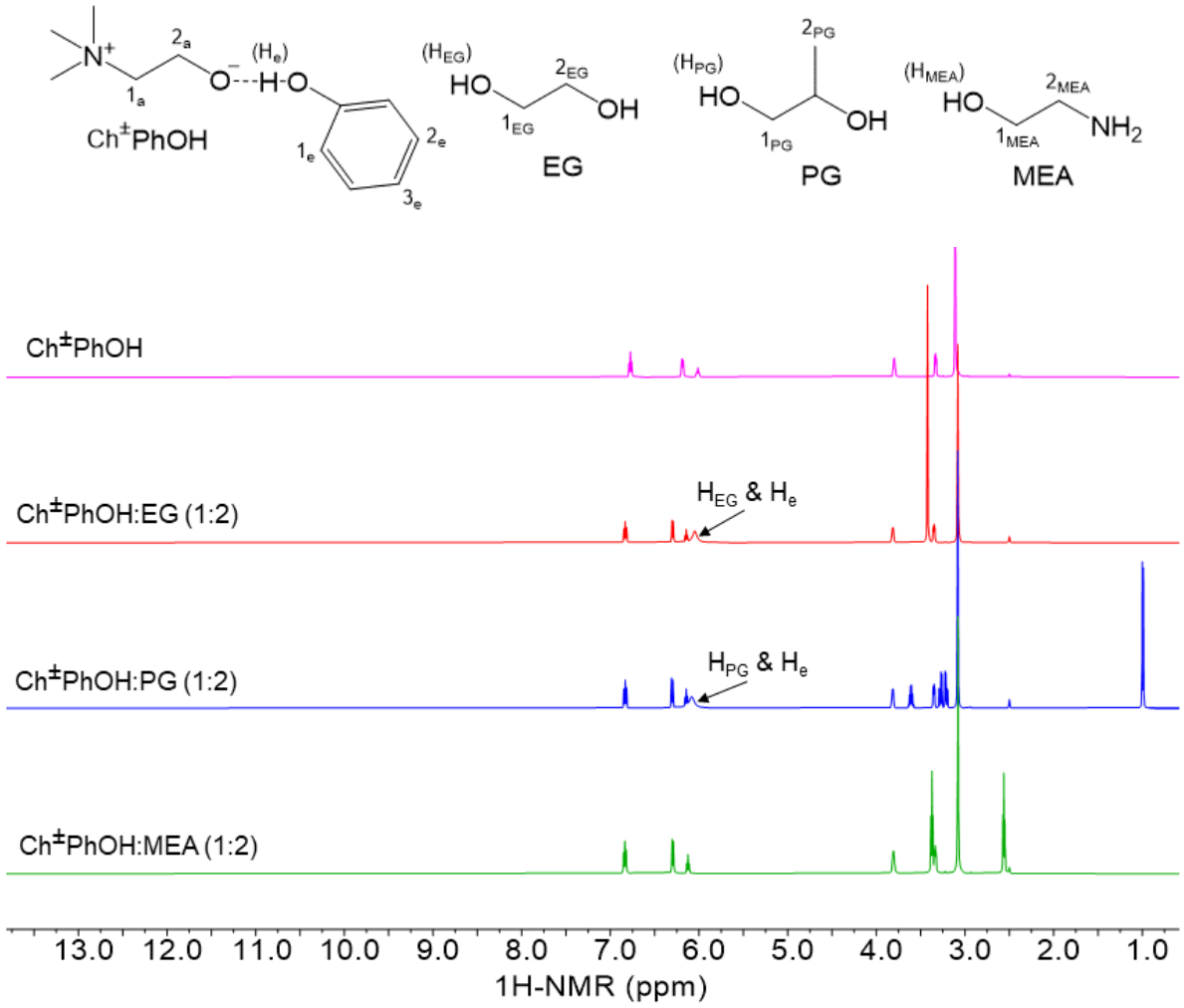

Figure S8. ^{1}H-NMR spectra of Ch±PhOH based eutectic solvents with EG, PG, and MEA HBDs in DMSO-d6.

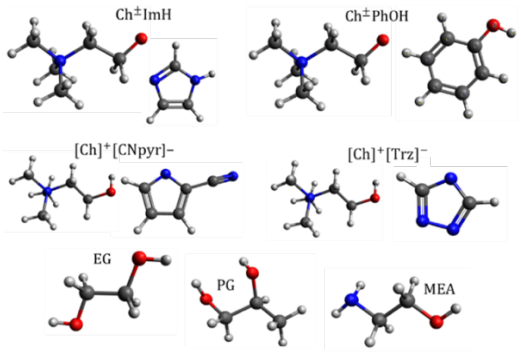

Figure S9. Structures and atom type notations of molecules simulated.

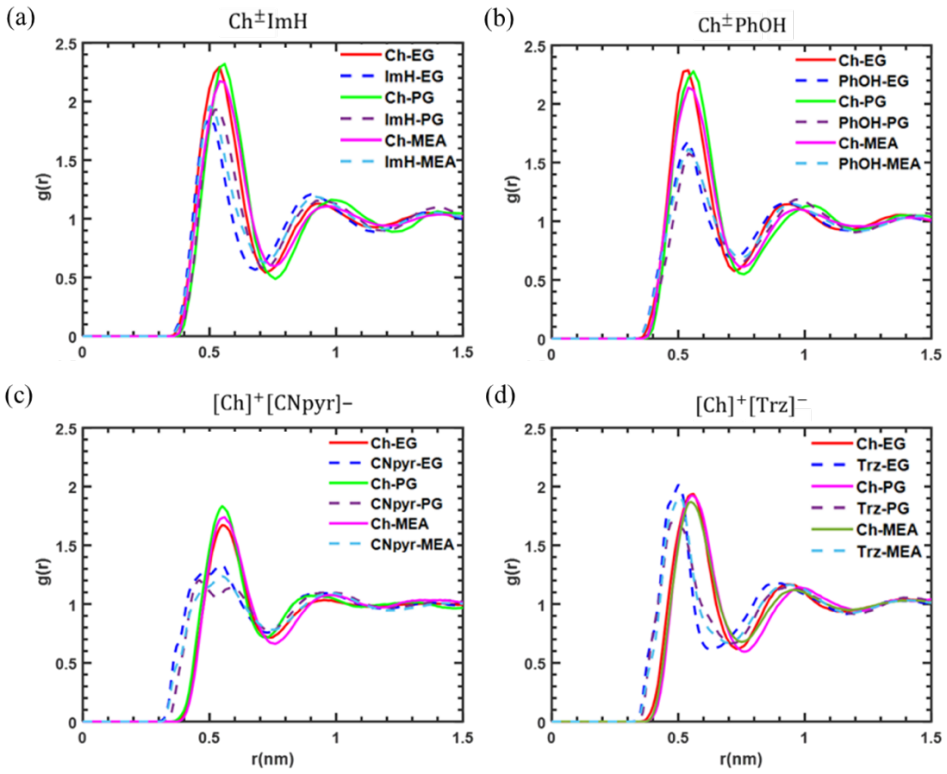

Figure S10. Center of mass (COM) radial distribution function (RDF) plots of $Ch^{\pm}ImH$ (a), $Ch^{\pm}PhOH$ (b), $[Ch]^{+}[CNpyr]^{-}$ (c), and $[Ch]^{+}[Trz]^{-}$ (d) based eutectic solvents with EG, PG, and MEA HBDs. Dotted and solid lines correspond to anion-HBD and cation-HBD interactions, respectively. Note that the stronger intensity in g(r) for $Ch^{\pm}ImH$ and $Ch^{\pm}PhOH$ maybe due to the unaccounted proton sharing observed experimentally.

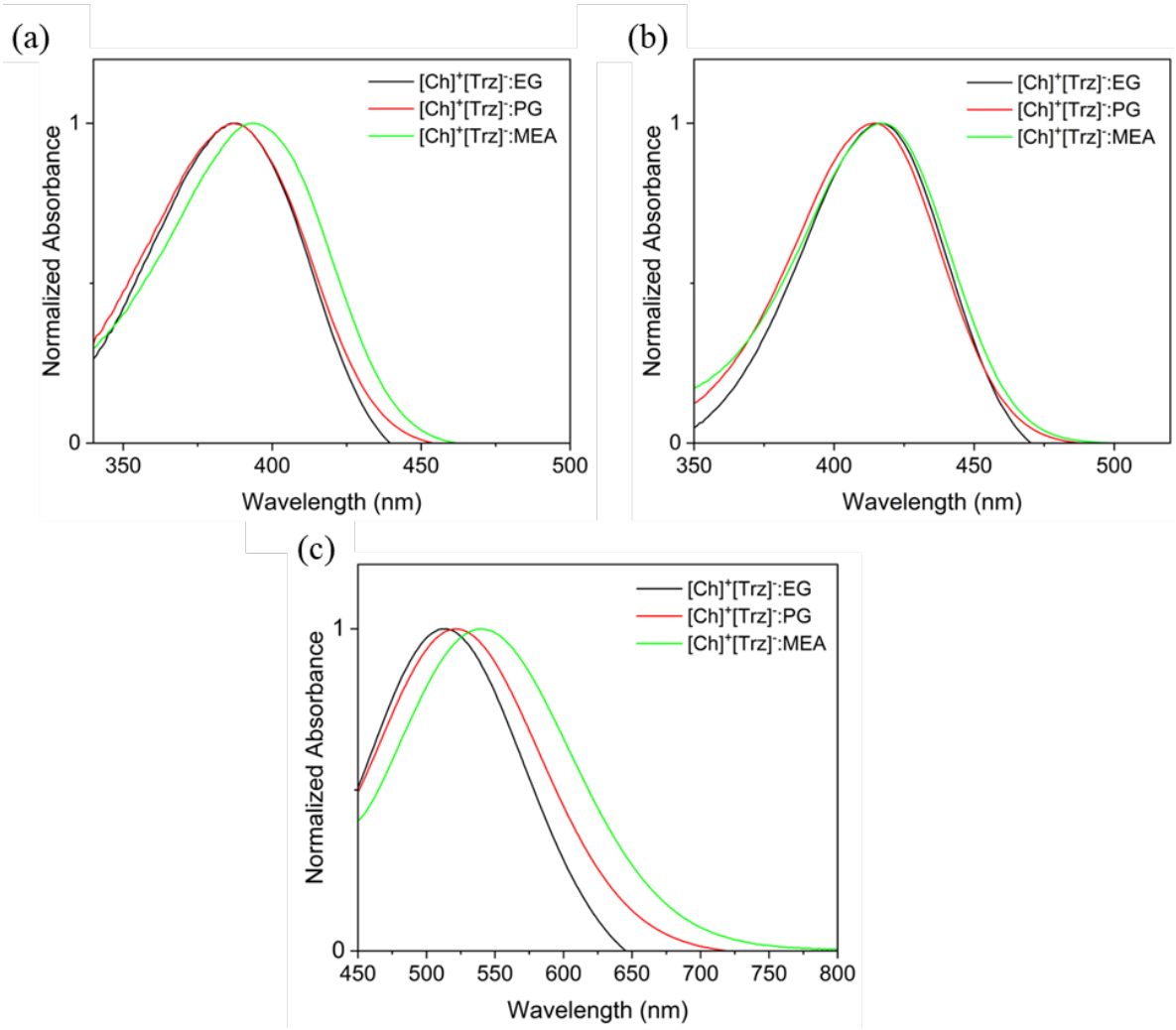

Figure S11. Normalized UV-vis absorbance spectra of 4-nitroaniline (a), N,N-diethyl-4-nitroaniline (b), and betaine 30 (c) dissolved in the $[Ch]^+[Trz]^-$ based eutectic solvents.

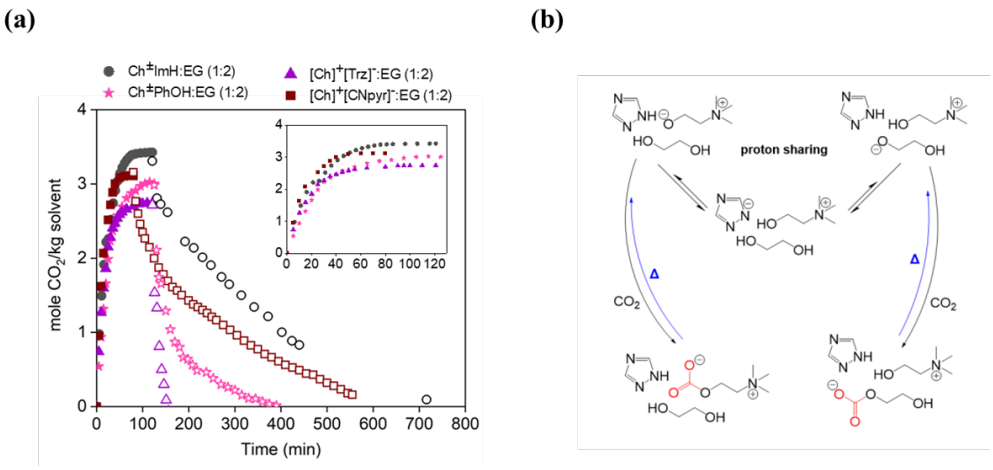

Figure S12. CO_2 absorption and desorption (a) and the chemisorption mechanism (b) in the EG based eutectic solvents as reported in Dikki *et al.*[1]. The filled symbols represent the absorption data at 1 bar CO_2 and 25 °C (see also the inset) and the hollow symbols represent the desorption data at 50 °C under N_2. The desorption temperature was elevated to 70 °C for the $Ch^{\pm}ImH$ based systems.

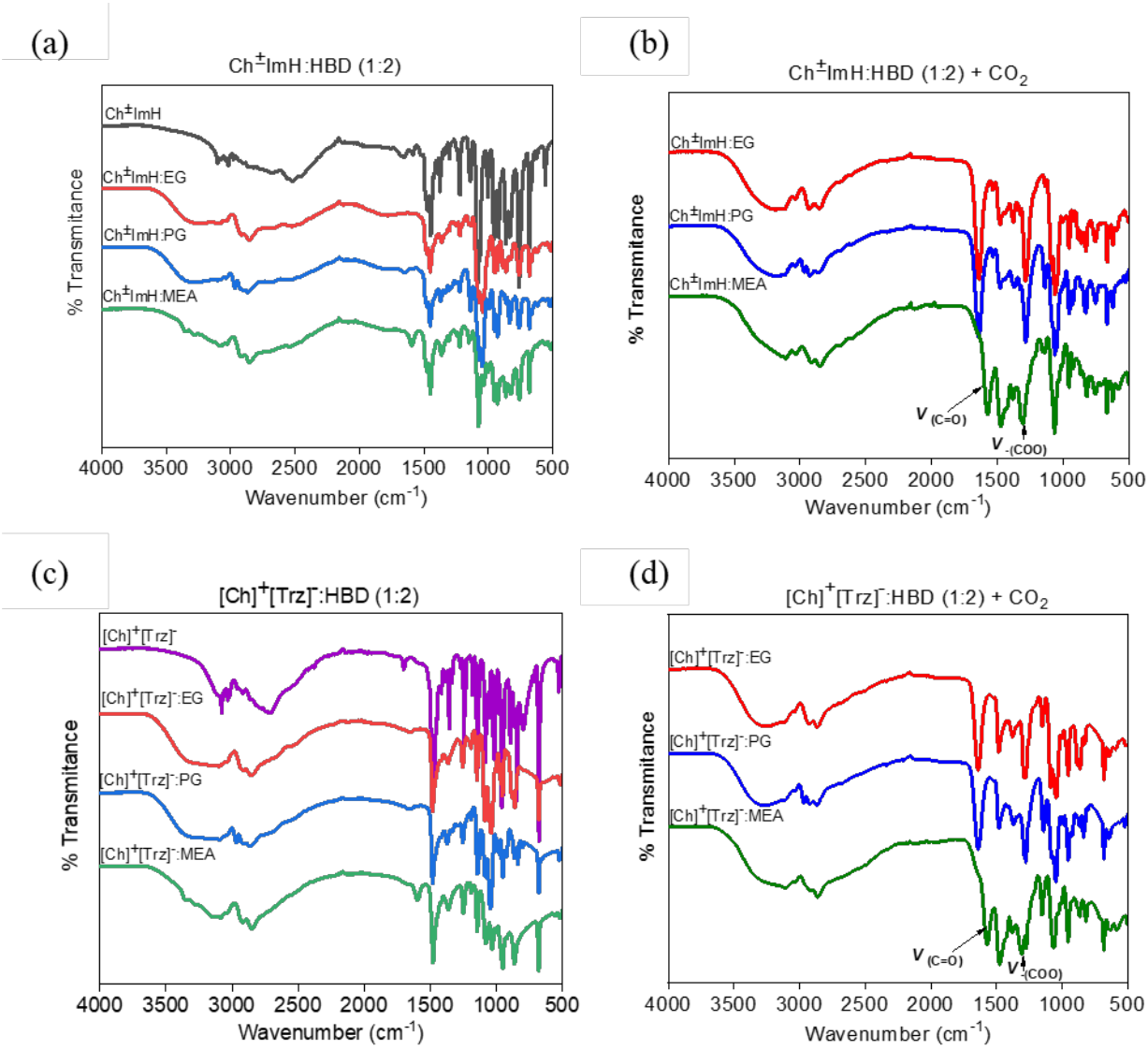

Figure S13. FTIR spectra of (a) neat and (b) CO_2 saturated of $Ch^{\pm}ImH$ based eutectic solvents, and (c) neat and (d) CO_2 saturated of $[Ch]^+[Trz]^-$ based eutectic solvents with EG, PG, and MEA HBDs.

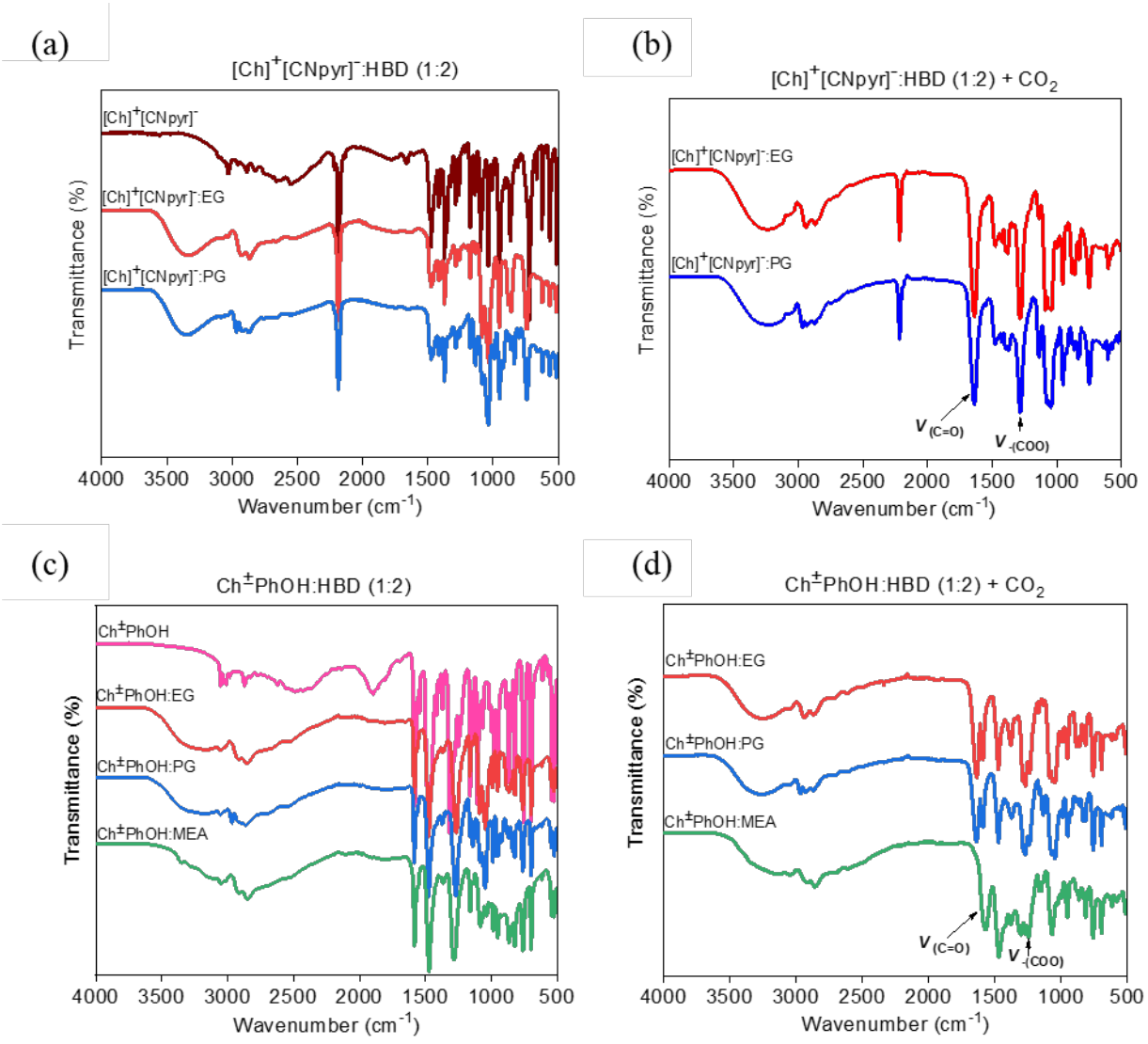

Figure S14. FTIR spectra of (a) neat and (b) CO_2 saturated $[Ch]^+[CNpyr]^-$ of based eutectic solvents, and (c) neat and (d) CO_2 saturated of $Ch^{\pm}PhOH$ based eutectic solvents with EG, PG, and MEA HBDs.

Table S6. Change in density with CO_2 saturation of the solvents at 1 bar CO_2 and 25 °C.

	Density before CO_2 saturation (g/cm^3)	Density after CO_2 saturation (g/cm^3)
$Ch^{\pm}$PhOH:EG (1:2)	1.10333	1.15101
$Ch^{\pm}$PhOH:PG (1:2)	1.06866	1.11384
$Ch^{\pm}$ImH:EG (1:2)	1.10043	1.16215
$Ch^{\pm}$ImH:PG (1:2)	1.06502	1.11996
$[Ch]^+[Trz]^-$:EG (1:2)	1.12096	1.17016
$[Ch]^+[Trz]^-$:PG (1:2)	1.08484	1.12598
$[Ch]^+[CNpyr]^-$:EG (1:2)	1.09477	1.15497
$[Ch]^+[CNpyr]^-$:PG (1:2)	1.06229	1.11743

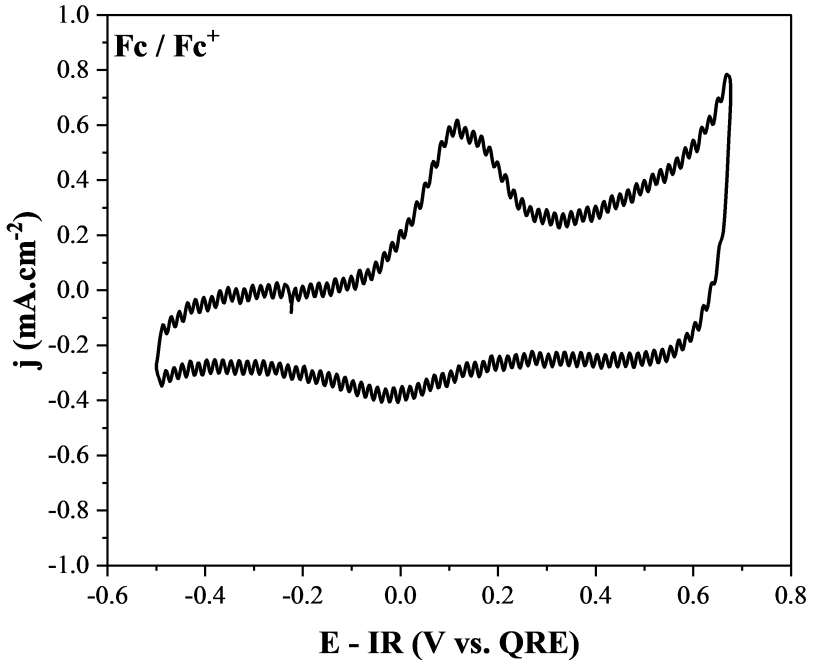

Figure S15. Cyclic voltammogram of Fc/Fc^+ redox couple on Pt micro electrode vs. Pt quasi reference electrode with 1000 $mV.s^{-1}$ scan rate

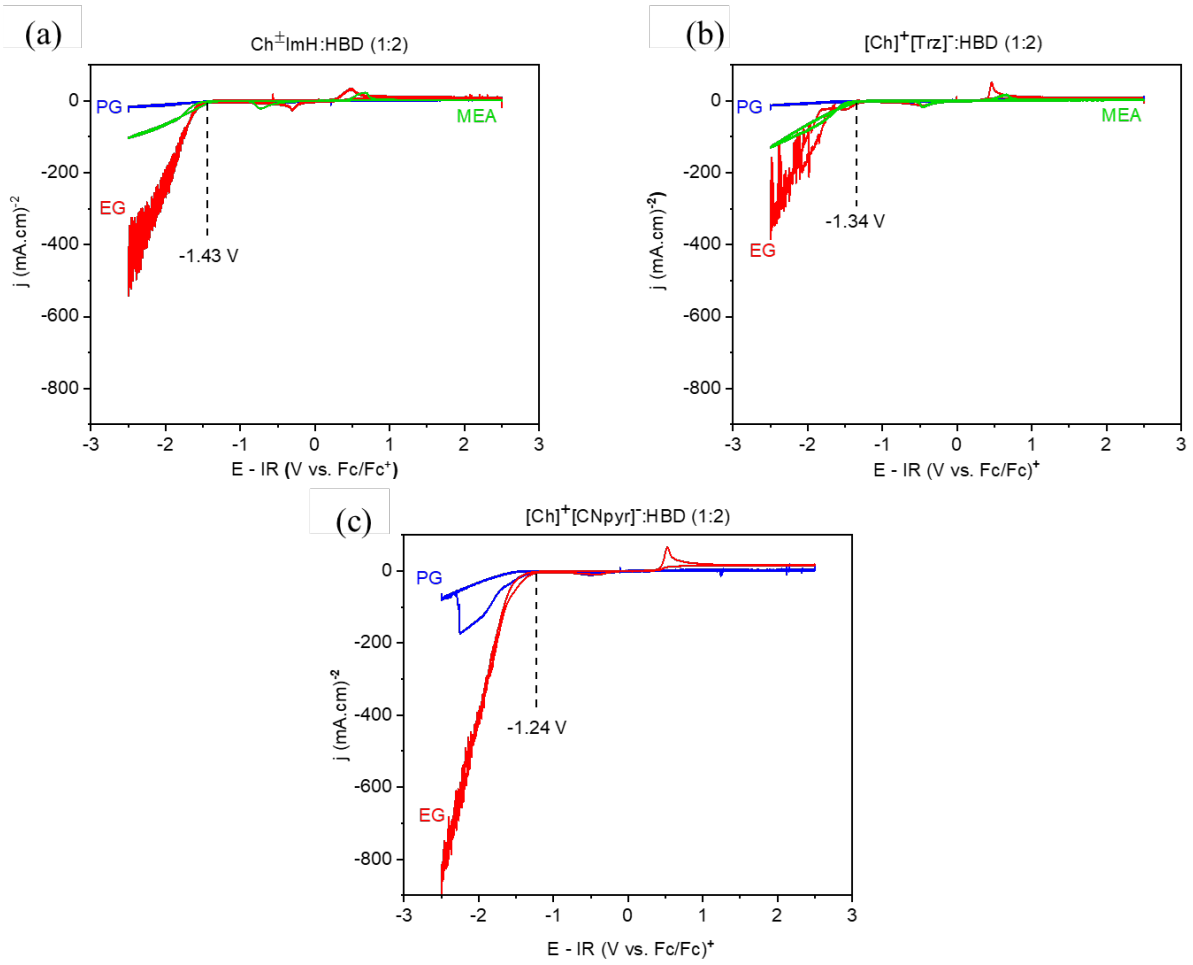

Figure S16. Cyclic voltammetry of $Ch^{\pm}ImH$ (a), $[Ch]^{+}[Trz]^{-}$ (b), and $[Ch]^{+}[CNpyr]^{-}$ (c) investigating their electrochemical window.

Table S7. Structural descriptors of the cations, anions, and diluents considered for QSPR analysis from this study.

HBAs	E HOMO (eV)	E LUMO (eV)	Dipole (debye)	CPK Area (Å²)	PSA (Å²)	CPK Volume (Å³)	CPK Ovality
$Ch^{\pm}$	-3.81	-1.15	12.73	151.27	15.364	127.98	1.23
$[Ch]^{+}$	-11.79	-4.2	3.65	154.27	19.796	129.91	1.24
ImH	-6.56	-0.51	3.84	93.86	20.399	74.06	1.1
PhOH	-6.48	-0.02	1.57	124.55	20.25	106.54	1.15
$[CNpyr]^{-}$	-0.82	4.88	3.55	117.81	23.848	98.14	1.14
$[Trz]^{-}$	-1.45	4.13	1.58	83.58	30.687	64.19	1.08
EG	-7.84	-0.44	2.28	91.57	40.454	66.76	1.15
PG	-7.76	-0.45	2.14	111.16	39.862	85.04	1.19
MEA	-6.77	-0.31	1.04	96.14	45.569	70.01	1.17

HBAs	Polarizability	HBD Count	HBA Count	ZPE (kJ/mol)	Sº (J/molº)	Hº (au)	Gº (au)	Cv (J/molº)
$Ch^{\pm}$	51.13	0	2	473.09	362.16	-328.13	-328.17	103.35
$[Ch]^{+}$	50.12	0	0	514.59	366.84	-328.58	-328.62	105.92
ImH	45.95	0	1	186.01	272.89	-226.21	-226.24	55.41
PhOH	48.49	1	1	272.54	315.64	-307.36	-307.40	80.18
$[CNpyr]^{-}$	47.98	0	2	176.42	308.3	-301.85	-301.89	72.47
$[Trz]^{-}$	45.26	0	3	120.37	267.29	-241.71	-241.74	45.78
EG	45.04	2	2	222.4	295.9	-230.24	-230.27	58.03
PG	46.54	2	2	295.08	322.78	-269.54	-269.58	74.04
MEA	45.53	1	2	255.4	299.11	-210.36	-210.39	61.04

Table S8. Structural descriptors of the cations, anions, and diluent considered for QSPR analysis from the literature.

	E HOMO (eV)	E LUMO (eV)	Dipole (debye)	CPK Area (Å²)	PSA (Å²)	CPK Volume (Å³)	CPK Ovality	Polarizability
$[EMIM]^+$	-11.91	-5.23	1.65	160.71	1.179	135.46	1.26	50.78
$[P_{2222}]^+$	-13.11	-3.81	0.64	220.73	0	191.47	1.37	54.71
$[N_{2222}]^+$	-13.57	-3.75	0.68	193.68	0	176.18	1.27	53.35
$[CNpyr]^-$	-0.82	4.88	3.55	117.81	23.848	98.14	1.14	47.98
$[1,2,3\ Trz]^-$	-1.46	3.83	3.81	83.33	35.139	63.76	1.08	45.29
$[Pro]^-$	-1.34	2.93	8.08	136.61	40.649	115.12	1.19	49.7
$[Im]^-$	-0.58	3.99	1.28	90.22	17.231	71.71	1.08	46.11
EG	-7.84	-0.44	2.28	91.57	40.454	66.76	1.15	45.04

	HBD Count	HBA Count	ZPE (kJ/mol)	S^o (J/mol^o)	H^o (au)	G^o (au)	Cv (J/mol^o)
$[EMIM]^+$	0	2	442.16	353.73	-344.460408	-344.500578	101.05
$[P_{2222}]^+$	0	0	700.98	436.18	-657.897013	-657.946545	150.64
$[N_{2222}]^+$	0	0	727	409.04	-371.233778	-371.280228	140.42
$[CNpyr]^-$	0	2	176.42	308.3	-301.854451	-301.889462	72.47
$[1,2,3\ Trz]^-$	0	3	118.17	262.31	-241.686755	-241.716542	47.5
$[Pro]^-$	0	3	342.79	338.74	-400.592313	-400.63078	90.06
$[Im]^-$	0	2	150.05	263.78	-225.652	-225.6823	50.91
EG	2	2	222.4	295.9	-230.240458	-230.27406	58.03

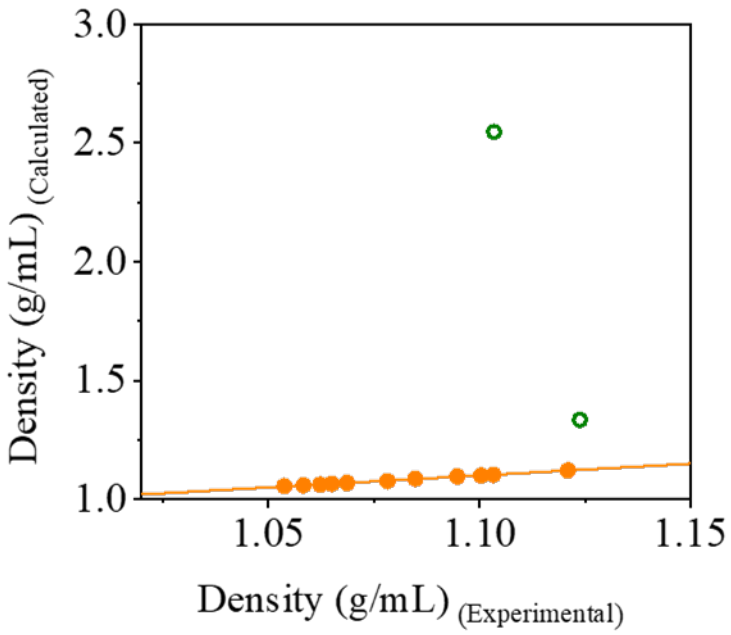

Figure S17. Comparison between experimental and predicted values of the density of the eutectic solvents. Hollow symbols represent comparison between experimental density data of eutectic solvents obtained from literature and predicted values by our model.

Multi-linear regression model (MLR) was performed for density to obtain the best fit linear model that correlates the identified descriptors of eutectic solvents along with regression parameters as expressed by eqn. S12:

$$Density_{(g/mL)} = -32.879 + 0.261 \times CPK\ volume_{cation} - 0.102 \times E\ LUMO_{anion} + 0.001 \times S^{o}_{anion} - 0.034 \times E\ HOMO_{diluent} - 0.002 \times CPK\ Area_{diluent} \quad \text{(S12)}$$

REFERENCES

(1) Dikki, R.; Cagli, E.; Penley, D.; Karayilan, M.; Gurkan, B. Formation of Choline Salts and Dipolar Ions for CO2 Reactive Eutectic Solvents. *Chem. Commun.* **2023**, *59* (80), 12027–12030. https://doi.org/10.1039/D3CC03272H.

(2) Evjen, S.; Wanderley, R.; Fiksdahl, A.; Knuutila, H. K. Viscosity, Density, and Volatility of Binary Mixtures of Imidazole, 2-methylimidazole, 2,4,5-Trimethylimidazole, and 1,2,4,5-Tetramethylimidazole with Water. *J. Chem. Eng. Data* **2019**, No. 64, 507−516. https://doi.org/10.1021/acs.jced.8b00674.

(3) Van Der Spoel, D.; Lindahl, E.; Hess, B.; Groenhof, G.; Mark, A. E.; Berendsen, H. J. C. GROMACS: Fast, Flexible, and Free. *J. Comput. Chem.* **2005**, *26* (16), 1701–1718. https://doi.org/10.1002/jcc.20291.

(4) Martinez, L.; Andrade, R.; Birgin, E. G.; Martinez, J. M. Packmol: A Package for Building Initial Configurations for Molecular Dynamics Simulations. *J. Comput. Chem.* **2009**, *30*, 2157–2164. https://doi.org/10.1002/jcc.

(5) Koziara, K. B.; Stroet, M.; Malde, A. K.; Mark, A. E. Testing and Validation of the Automated Topology Builder (ATB) Version 2.0: Prediction of Hydration Free Enthalpies. *J. Comput. Aided. Mol. Des.* **2014**, *28* (3), 221–233. https://doi.org/10.1007/s10822-014-9713-7.

(6) Evans, D. J.; Holian, B. L. The Nose-Hoover Thermostat. *J. Chem. Phys.* **1985**, *4074*, 4069–4074.

(7) Saito, H.; Nagao, H.; Nishikawa, K.; Kinugawa, K. Molecular Collective Dynamics in Solid Para-Hydrogen and Ortho-Deuterium: The Parrinello–Rahman-Type Path Integral Centroid Molecular Dynamics Approach. *J. Chem. Phys.* **2003**, *119* (2), 953–963. https://doi.org/10.1063/1.1578474.

(8) Schmid, N.; Eichenberger, A. P.; Choutko, A.; Riniker, S.; Winger, M.; Mark, A. E.; Van Gunsteren, W. F. Definition and Testing of the GROMOS Force-Field Versions 54A7 and 54B7. *Eur. Biophys. J.* **2011**, *40* (7), 843–856. https://doi.org/10.1007/s00249-011-0700-9.

(9) Hess, B.; Bekker, H.; Berendsen, H. J. C.; Fraaije, J. G. E. M. LINCS: A Linear Constraint Solver for Molecular Simulations. *J. Comput. Chem.* **1997**, *18* (12), 1463–1472. https://doi.org/10.1002/(SICI)1096-987X(199709)18:12<1463::AID-JCC4>3.0.CO;2-H.

(10) Curme Jr, G. O.; Young, C. O. Ethylene Glycol: A Contribution of Chemistry to the Automobile Antifreeze Problem. *Ind. Eng. Chem.* **1925**, 1117–1120.

(11) He, F.; Wu, N.; Zhou, Z.; Wang, J. Experimental Investigation on Transpiration Cooling Using Propylene Glycol Aqueous Solution. *Int. J. Therm. Sci.* **2021**, *164*, 106890. https://doi.org/10.1016/j.ijthermalsci.2021.106890.

(12) Jadhav, P. D.; Chatti, R. V; Biniwale, R. B.; Labhsetwar, N. K.; Devotta, S.; Rayalu, S. S. Monoethanol Amine Modified Zeolite 13X for CO2 Adsorption at Different Temperatures. *Energy & Fuels* **2007**, No. 21, 3555–3559.